Materials Today Communications 25 (2020) 101517

Contents lists available at ScienceDirect

Materials Today Communications

journal homepage: www.elsevier.com/locate/mtcomm

# Theoretical studies of $CsSnX_3$ (X = Cl, Br and I) for energy storage and hybrid solar cell applications

Liaqat Ali[a,b], Murad Ahmad[a,b], Muhammad Shafiq[c], Tahir Zeb[d], Rashid Ahmad[e], M. Maqbool[f], Iftikhar Ahmad[a,g], S. Jalali-Asadabadi[h], Bin Amin[c,*]

[a] Center for Computational Materials Science, University of Malakand, Pakistan
[b] Department of Physics, University of Malakand, Chakdara, Pakistan
[c] Department of Physics, Abbottabad University of Science and Technology, Abbottabad 22010, Pakistan
[d] Department of Physics, Abdul Wali Khan University Mardan, Pakistan
[e] Department of Chemistry, University of Malakand, Chakdara, Pakistan
[f] Department of Clinical & Diagnostic Sciences, The University of Alabama at Birmingham, Birmingham, AL 35294, USA
[g] Gomal University, DI Khan, Pakistan
[h] Department of Physics, Faculty of Sciences, University of Isfahan, Hezar Gerib Avenue, Isfahan 81746-73441, Iran

ARTICLE INFO

*Keywords:*
Perovskites
Photovoltaic
Structural
Electronic
Optical
DFT

ABSTRACT

Perovskites $CsSnX_3$ (X = Cl, Br and I) are promising for photovoltaic cells and other energy store devices, having high stability and less toxicity (lead free). The present work explored the structural, electronic and optical properties of these perovskites in different phases using generalized gradient approximation (GGA) and modified Becke-Johnson (TB-mBT) techniques. The structural properties of this system depend on temperature variation and selection of halogens, which changes the electronic and optical properties. The calculated structural parameters (lattice constants, bulk modulus, volume, bond length and bond angles) are in good agreement with the experimental values. The results presented in this article confirm that these compounds have direct band gaps, lie in the visible region (1.3–2.9 eV), hence they are more suitable candidates for optoelectronic devices. This study covers the lack of theoretical work concerned to these systems.

## 1. Introduction

Supply of clean energy for industrial and household uses is a main challenge of the present-day science and technology. Limited natural resources of oil and gas are running out with time and they also causing environmental pollution. Therefore, modulation from nonrenewable, i.e., fossil fuel to renewable energy resources is essential [1] as well as more efficient and cheap renewable energy resources are required for high photovoltaic applications.

Efficient materials for the conversion of solar energy into electrical energy are mostly perovskites such as $CsSnX_3$ (X = Cl, Br and I). Because of the direct band gaps semiconducting nature [9] these compounds have strong photovoltaic applications and can be used to construct high performance solar cells [2–6] as well as host materials for hybrid solar cells [7–10]. These compounds consist of one anion (X) at the face centers and two cations Cs and Sn at the corners and at the center of the cubic unit cells, respectively [10]. These perovskites also exist in other phases like, tetragonal, orthorhombic and monoclinic at different temperatures.

$CsSnX_3$ based solar cells are more stable and less toxic because of the Sn element [11]. Replacing Cs by an organic–inorganic compound such as $CH_3NH_3$ or $NH_2CH=NH_2$ in $CsSnX_3$ transforms it into organic-inorganic Tin halide perovskites and can be used as an active material for hybrid solar cells. In these materials p–p optical transition is favorable because Sn atom is a divalent atom and it does not lose its electrons in the 5s state. Hence, p states of the Sn atom strongly hybridize with the p states of halogens. Therefore, the lower part of the conduction bands of organo-tin-halides are made up from the unoccupied 5p orbitals of tin atoms, while the top of the valence bands contains mainly the halogen p orbitals mixed with 5s orbitals of tin atoms [12].

In these perovskites, $CsSnI_3$ exists in orthorhombic, tetragonal and cubic phases [13], and has strong photoluminescence, as well as possess high p-type electrical conductivity and high hole mobility [14]. They can be used as photodetectors [15,16] and semiconducting channel in thin film field effect transistors [17]. $CsSnBr_3$ has cubic structure at

* Corresponding author.
*E-mail address:* binukhn@aust.edu.pk (B. Amin).

https://doi.org/10.1016/j.mtcomm.2020.101517
Received 13 April 2020; Received in revised form 27 July 2020; Accepted 27 July 2020
Available online 23 August 2020

**Table 1**
Comparison of presently calculated, experimental and other theoretically calculated structural parameters of $CsSnX_3$ (X = Cl, Br and I) in cubic phase. The experimental results, when available, are reported in parentheses.

| Parameters | $CsSnCl_3$ | | $CsSnBr_3$ PBEsol | | $CsSnI_3$ | |
|---|---|---|---|---|---|---|
| | Present (Exp) | Others | Present (Exp) | Others | Present (Exp) | Others |
| *a* (Å) | 5.55 (5.56)[a] | 5.601[b], 5.49[c] | 5.792 (5.795)[e] | 5.807[f], 5.709[c] | 6.218 (6.219)[i] | 6.23[b], 6.14[c] |
| *V* (Å)$^3$ | 170.9 (172)[a] | 176[b], 165.5[c] | 194.31 (194.6)[e] | 195[f], 186.07[c] | 240.4 (241)[i] | 242[b], 231.48[c] |
| *B* (GPa) | 27 | 27.68[c] | 22 | 22.74[g], 25.19[c] | 18.21 | 18.33[j], 17.59[c] |
| $E_o$ (Ry) | −30,692.51 | −30,703.5[c] | −43,557.12 | −43,572.1[c] | −70,624.02 | −70,645.8[c] |
| *Bond length (Å)* | | | | | | |
| Cs-X | 4.03 | – | 4.104 | – | 4.269 | 4.334[b] (4.064)[i] |
| Sn-X | 2.8 | 2.8[d] | 2.9 (2.9)[h] | 2.94[d] | 3.11 (3.11)[i] | 3.136[b], 3.14[d] |
| Cs-Sn | 4.93 | – | 5.026 | – | 5.47 | – |
| *Bond angle* | | | | | | |
| X-Cs-X | 60° | – | 60° | – | 60° | – |
| X-Sn-X | 90° | (90°)[b] | 90° (90°)[h] | | 90° (90°)[k] | |
| Sn-Cs-X | 35.26° | – | 35.26° | – | 35.26° | – |
| *PBE* | | | | | | |
| *a* (Å) | 5.62 | | 5.81 | | 6.27 | |
| *V* (Å)$^3$ | 177 | | 196 | | 246 | |
| *B* (GPa) | 29 | | 23.54 | | 20 | |
| *LDA* | | | | | | |
| *a* (Å) | 5.51 | | 5.669 | | 6.131 | |
| *V* (Å)$^3$ | 168.3 | | 182 | | 230.4 | |
| *B* (GPa) | 22 | | 19.2 | | 17 | |

a = [20], b = [19], c = [24], d = [42], e = [43], f = [44], g = [45], h = [46], i = [47], j = [48], k = [8].

**Table 2**
Comparison of presently calculated, experimental and other theoretically calculated structural parameters of $CsSnX_3$ (X = Cl, Br and I) in tetragonal phase. The experimental results, where available, are reported in parentheses.

| Parameters | $CsSnBr_3$ PBEsol | | $CsSnI_3$ | |
|---|---|---|---|---|
| | Present (Exp) | Others | Present (Exp) | Others |
| *a* (Å) | 11.59 (11.59)[a] | – | 8.775 (8.772)[d] | 8.772[e] |
| *b* (Å) | 11.61 (11.61)[a] | – | 6.271 (6.261)[c] | 6.261[e] |
| *V* (Å)$^3$ | 1559 (1559)[a] | – | 482.87 (481)[c] | 481[e] |
| *B* (GPa) | 5.50 | – | 15.71 | 17.45[f] |
| $E_o$ (Ry) | −87,113.09 | – | −141,307.08 | – |
| *Bond length (Å)* | | | | |
| Cs_X | 5.79, 5.75 | – | 4.386, 4.82 | 4.27, 4.80[f] |
| Sn_X | 3.305, 2.64 (3.306, 2.67)[b] | 3.1, 3.7[c] | 3.102, 3.11 (3.095, 3.099)[g] | 3.136, 3.115[e] |
| Cs_Sn | 8.20, 8.46 | – | 5.38, 5.75 | – |
| *Bond angle* | | | | |
| X1-Cs-X2 | 90°, 180° | – | 90°, 180° | – |
| Sn-X1- Sn | 162° | 162°[b] | 161.82° (161.9°)[d] | 162°[e] |
| Sn-Cs-X1 | 90° | – | 90° | – |
| *PBE* | | | | |
| *a* (Å) | 11.60 | | 8.772 | |
| *b* (Å) | 11.59 | | 6.30 | |
| *V* (Å)$^3$ | 1562 | | 484 | |
| *B* (GPa) | 6.23 | | 24 | |
| *LDA* | | | | |
| *a* (Å) | 11.59 | | 8.60 | |
| *b* (Å) | 11.60 | | 6.14 | |
| *V* (Å)$^3$ | 1558 | | 454 | |
| *B* (GPa) | 2.67 | | 5.28 | |

a = [49], b = [50], c = [51], d = [47], e = [19], f = [48], g = [8].

room temperature, tetragonal phase below 292 K [9], and transits to orthorhombic phase at 80 K [13]. $CsSnCl_3$ exists in monoclinic, cubic and orthorhombic phases at room, high and low temperatures, respectively [18]. Scaife et al. [19] and Mauersberger and Huber [20] synthesized $CsSnI_3$ and studied its structural properties. Electrical conductivity and optical properties of $CsSnBr_3$ have been investigated in Ref. [21]. Fan et al. and Ghosh et al. experimentally studied the different properties of $CsSnX_3$ nanocrystals [22,23]. Density functional theory have been used to investigate the binding energy, phonon spectra, electronic band structure, optical and thermoelectric properties of $CsSnX_3$ [24–26].

Cubic phase of these compounds have been extensively investigated [27–29]. In this respect, it is surprising that rather than the structural properties of the orthorhombic phase of $CsSnBr_3$ and $CsSnCl_3$ no other theoretical investigation has been reported. Therefore, this system needs extensive theoretical and experimental studies to investigate their physical properties especially electronic and optical properties because of their applications in the optoelectronic devices. Present work explored the structural, electronic and optical properties of different phases of $CsSnX_3$. This study covers the lack of theoretical work concerning these properties.

## 2. Computational details

We employed density functional theory (DFT) using WIEN2k code [30]. Generalized gradient approximation (GGA) [31] is used to optimize lattice constants and explore the structural properties. To calculate optical and electronic properties regular and non-regular Tran and Blaha Becke-Johnson (TB-mBJ and nTB-mBJ) exchange potentials are used [32,33]. In nTB-mBJ the electron density is optimized for each compound. The muffin-tin radii are selected as 2.5, 2.36, 1.70, 2.5 and 2.3Mauersberger80a.u. for Cs, Sn, Br, I and Cl, respectively. A 58 × 58 × 58 k-mesh is used for integrating the Brillouin zone in cubic phase and 25 × 25 × 25 k-grid for tetragonal and orthorhombic phases.

## 3. Results and discussion

Structural phase transition as function of temperature is observed in $CsSnX_3$ (X = Cl, Br, I), i.e., they have cubic, tetragonal and orthorhombic unit cells, because their lattice parameters are different and so their cubic cells are different, as well. These unit cells are characterized by distortion and tilting produced in the octahedron of $CsSnX_3$. At low temperatures, the distortion produced in the octahedron of these perovskites is due to the lone pair electron of Sn atoms [34]. Structural variations also depend on the selection of X (X = Cl, Br and I), which

**Table 3**
Comparison of presently calculated, experimental and other theoretically calculated structural parameters of $CsSnX_3$ (X = Cl, Br and I) in orthorhombic phase. The experimental results, where available, are reported in parentheses.

| Parameters | $CsSnCl_3$ | | $CsSnBr_3$ PBEsol | | $CsSnI_3$ | |
|---|---|---|---|---|---|---|
| | Present (Exp) | Others | Present (Exp) | Others | Present (Exp) | Others |
| *a* (Å) | 10.328 (10.328)[a] | – | 8.2149 (8.2149)[c] | – | 8.677 (8.688)[f] | 8.738[b] |
| *b* (Å) | 17.623 (17.677)[a] | – | 11.6321 (11.6322)[c] | – | 8.632 (8.643)[f] | 8.730[b] |
| *c* (Å) | 4.765 (4.765)[a] | – | 8.1523 (8.1844)[c] | – | 12.365 (12.377)[f] | 12.528[b] |
| *V* (Å)$^3$ | 867.3 (870)[a] | – | 779.01 (782.08)[c] | – | 926 (929)[f] | 955[c] |
| *B* (GPa) | 3.65 | – | 13.93 | – | 17 (19.89)[g] | 15.92[h] |
| $E_o$ (Ry) | −122,769.41 | – | −174,227.97 | – | −282,496.06 | – |
| *Bond length* (Å) | | | | | | |
| Cs_X | 3.78, 4.26 | – | 3.89, 4.75 | – | 4.064, 3.96 (4.064, 3.97)[h] | 3.84, 3.86, 3.93[h] |
| Sn_X | 2.85, 2.94 | 2.84, 2.85[d] | 2.83, 2.89 (2.82, 2.88)[e] | 2.97,2.98[d] | 3.10, 3.12 (3.10, 3.120)[f] | 3.17, 3.18 3.19[d] |
| Cs_Sn | 5.17. 5.026 | – | 5.21, 5.75 | – | 5.26, 5.02 | – |
| *Bond angle* | | | | | | |
| X-Cs-X | 93.8° | – | 90.65° | – | 170° | – |
| Sn-X- Sn | 90° | 90°[b] | 172° (172°)[e] | – | 172.3° (172.3°)[f] | 173[b] |
| Sn-Cs-X | 83.23 | – | 93.67° | – | 91.43° | – |
| *PBE* | | | | | | |
| *a* (Å) | 10.68 | | 8.2177 | | 8.688 | |
| *b* (Å) | 17.308 | | 11.6321 | | 8.643 | |
| *c* (Å) | 4.765 | | 8.5936 | | 12.44 | |
| *V* (Å)$^3$ | 880.8 | | 821.46 | | 934 | |
| *B* (GPa) | 5.43 | | 16.45 | | 23 | |
| *LDA* | | | | | | |
| *a* (Å) | 10.018 | | 8.2177 | | 8.688 | |
| *b* (Å) | 17.146 | | 11.6321 | | 8.40 | |
| *c* (Å) | 4.765 | | 8.3561 | | 12.00 | |
| *V* (Å)$^3$ | 819 | | 798.48 | | 876 | |
| *B* (GPa) | 3.58 | | 10.67 | | 15.23 | |

a = [20], b = [19], c = [52], d = [42], e = [50], f = [47], g = [48], h = [53].

can change the electronic structure and optical properties of $CsSnX_3$. Ground state energies of optimized volumes of the unit cells of each compound are presented in tables, which show that the cubic phase of these compounds is stable, in agreement with Ref. [35]. Changing anion from Cl to Br and to I enhances Coulombic attractions between electrons and nuclei, which decrease ground state energies.

Structural parameters such as lattice constants, bulk moduli, volumes, bond lengths and bond angles of these compounds are calculated using local density approximation (LDA), Perdew, Burke and Ernzerhof potentials, i.e., PBE and PBEsol with Birch-Muranghan equation of state [36]. These values are compared with available experiments and other calculations, presented in tables. It is clear from Table 1 that LDA results underestimated the volumes of the cubic phase by 1.74–6.47%, tetragonal phase by 0.064–5.61% and orthorhombic phases by 2.097–5.86%. The volumes obtained by PBE are overestimated for cubic by 0.72–2.90%, tetragonal by 0.192–0.62% and orthorhombic by 0.54–5.03%. The volume mismatching of about 0.15–0.61% for cubic phases, 0.00–0.388% for tetragonal phases and 0.31–0.39% for the orthorhombic phases of $CsSnX_3$ are found using PBEsol, given in Tables 1 – 3.

In cubic and orthorhombic phases, an increase in volumes are investigated by changing anion from Cl to Br and to I, due to increase in the atomic size, while in the case of the tetragonal phase these values decrease, respectively. It is also found that bulk modulus (B) decreases from Cl to Br and to I for cubic phase. This shows that the compressibility and hardness of these compounds decrease by changing the anions, while for tetragonal and orthorhombic phases its order changes, i.e., bulk modulus decreases from I to Br and to Cl. This shows that the orthorhombic and tetragonal phases of $CsSnX_3$ are harder than the other phases. The calculated bond lengths and bond angles are in good agreement with the available experimental and theoretical values. An increase in the bond lengths from Cl to Br to I is due to the increase in size of anions. Structural parameters calculated by using PBEsol are in good agreement with the experimental values, see Fig. 1.

### 3.1. Electronic properties

Electronic band structure and band gap energy of a compound provide a key factor to understand the optical behavior and excitons transition for the technological applications of a compound. The calculated band structures of $CsSnX_3$ using non-regular Tran and Blaha modified Becke-Johnson approach (nTB-mBJ) are presented in Fig. 2. For all cubic $CsSnX_3$ systems, conduction band minima (CBM) and valence band maxima (VBM) are located at R symmetry position, while for tetragonal and orthorhombic phases VBM and CBM are located at Γ symmetry point. Hence, all these materials are direct band gap semiconductors, and lie in the visible range of the spectrum [37,38].

Replacing Cl by Br and I in $CsSnX_3$ (X = Cl, Br and I) decreases the band gap. This decrease in the band gap is due to the fact that the heavier atoms (Br and I) have more charge carriers (free electrons and holes) than Cl which increase the number of charge carriers in their respective energy bands. Hence, states near the Fermi level ($E_F$) become occupied and conduction bands shift towards the Fermi level ($E_F$). Furthermore, this increases the lattice constants and bond lengths as well as the couplings between Cs-d, Sn-p and I/Br/Cl-p orbitals, which the later in turn can cause to reduce the splitting between bonding and anti-bonding levels and thereby the bandgap. Calculated values of the bandgaps using PBEsol, TB-mBJ and nTB-mBJ approaches are presented in Table 4. These values show that PBEsol and TB-mBJ underestimate the band gaps, while the nTB-mBJ approach is consistent with experiments.

### 3.2. Density of states

To analyze the behavior of band structures and the contributions of core and valence electrons, the partial density of states (PDOS) are

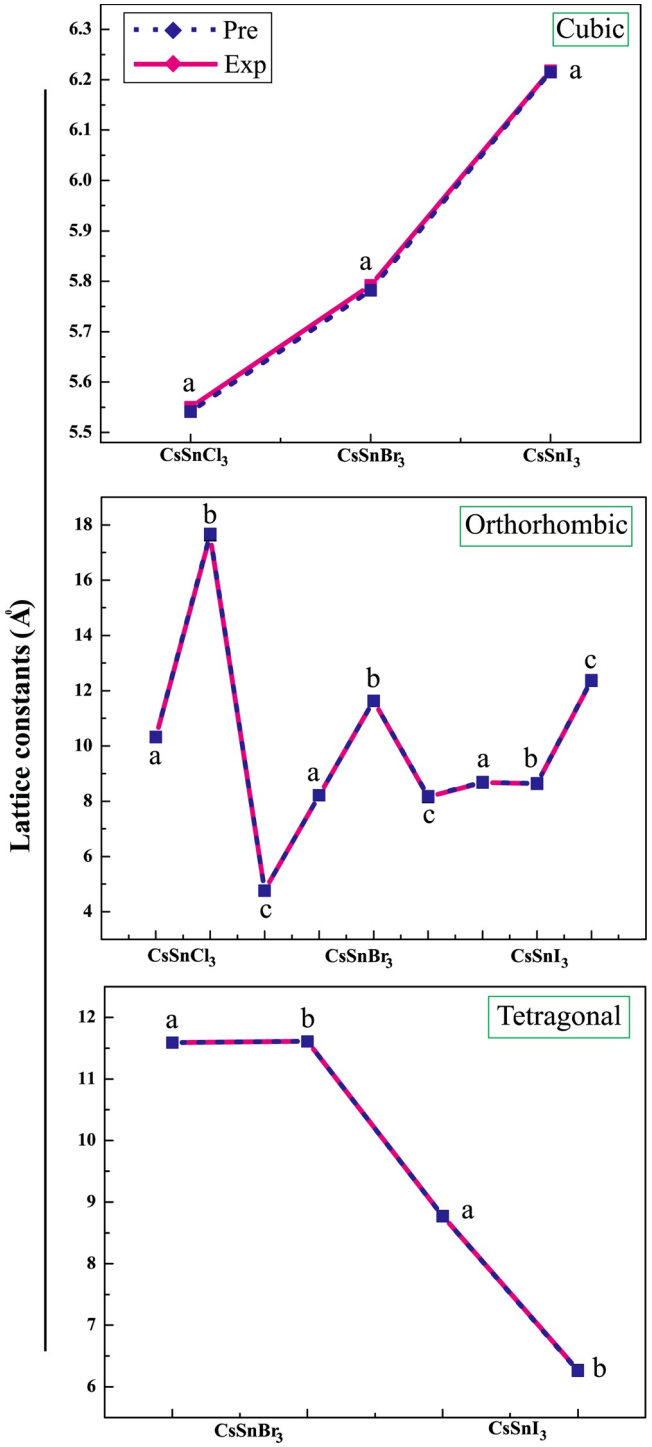


**Fig. 1.** Presently PBEsol calculated versus experimental lattice constant curves for cubic, tetragonal and orthorhombic phases of $CsSnX_3$ (X = Cl, Br and I).

investigated and presented in Fig. 3 The first row of figure represents the cubic, orthorhombic and tetragonal phases of $CsSnI_3$ respectively. Figure shows that the major contribution in the valence band of all the phases are due to the Sn-s, I-p, Cs-p, $I_1$-p and $I_2$-p states, while in the conduction bands it is due to the Cs-d, Sn-p, $I_1$-p states respectively.

Second row of the figure represents the PDOSs of the cubic, orthorhombic and tetragonal phase of $CsSnBr_3$ respectively. Sn-s and Br-p states contribute in the valence bands at −17 to −5 eV, while conduction bands originate from Sn-p and Br-p states at 1.8–5.5 eV of the cubic $CsSnBr_3$. Valence band of orthorhombic $CsSnBr_3$ is due to the Cs-p, $Br_1$-p and Sn-p at −9.5 to 3.0 eV, while conduction band is due to the Cs-d, Sn-p and $Br_2$-p states. In case of tetragonal $CsSnBr_3$, valence band consist of $Br_1$-p, Cs-p, Sn-s and Sn-p states, whereas the dominant states in the conduction bands are Cs-d, Sn-p and $Br_2$-p states.

Bottom row of the figure represents PDOSs for cubic and orthorhombic phases of $CsSnCl_3$. In cubic phase of $CsSnCl_3$, valence band is due to the Cl-p, Sn-s and Sn-p states, while conduction band is due to the Sn-p and Cl-p states. For orthorhombic $CsSnCl_3$, valence band comprises of Sn-s, $Cl_1$-p, Cs-p and $Cl_2$-p states, while conduction band is dominated by Cs-d, Sn-p, $Cl_1$-p states.

To investigate the binding nature of these compounds electronic charge densities are explored in (100) and (110) planes, see Fig. 4. Charge distribution in (100) plane shows existence of the ionic bonds between Cs and halide ions, while in (110) plane shows the existence of covalent bonds between Sn and hallide ions. The main reason for the covalent nature of bonding is the hybridization between Cs-d and Sn-p states.

## 4. Optical properties

$CsSnX_3$ (X = Cl, Br and I) compounds are direct band gap semiconductors and suitable for optoelectronic applications. Therefore, the optical parameters, such as energy loss function $L(\omega)$, dielectric function $\epsilon(\omega)$, refractive index $n(\omega)$, and sum rule $N_{\text{eff}}(\omega)$ are investigated by nTB-mBJ approach.

The dielectric function $\epsilon(\omega) = \epsilon_1(\omega) + \iota\epsilon_2(\omega)$ where $\epsilon_1(\omega)$ and $\epsilon_2(\omega)$ are the real and imaginary parts, is presented in Fig. 5. Moreover, $\epsilon_1(\omega)$ yields the electric polarizability of the material. Zero energy limit of $\epsilon_1(\omega)$ explores the electronic part of static dielectric constant. Fig. 5 shows strong dependency of $\epsilon_1(\omega)$ on the optical band gaps of these compounds, in agreement with Penn model [39].

The calculated values of $\epsilon_1(\omega)$ for orthorhombic and cubic phases of $CsSnCl_3$ are 3.1 and 2.5, for cubic, orthorhombic and tetragonal phases of $CsSnBr_3$ are 3.2, 6.3 and 4.1, while for cubic, orthorhombic and tetragonal phases of $CsSnI_3$ are 5.8, 5.9 and 4.5 respectively. Its value increases to maximum and then goes to negative at about 19.67–22 eV. It shows that the incident photon beam will be attenuated or totally reflected from the material and has metallic nature, otherwise dielectric [40]. At photon energies of 2.5, 1.35 and 2.0 eV the peak values of $\epsilon_1(\omega)$ are observed for cubic, orthorhombic and tetragonal phase of $CsSnBr_3$, respectively. It has negative values for cubic phase of $CsSnBr_3$ at 18–22 eV, for tetragonal at 16–20 eV and for orthorhombic at 14.3–14.7 eV. For cubic phase of $CsSnI_3$, however, its negative value lies at 2.5 eV and at higher energies for other phases, which can be attributed to the metallic behavior, see Fig. 5.

Imaginary part of the dielectric function $\epsilon_2(\omega)$ reveals the amount of energy absorbed by a material to produce electrons and holes are calculated and presented in Fig. 5. The energies at critical points for orthorhombic and cubic phases are 1.9 and 2.9 eV, yielding the optical band gap of $CsSnCl_3$ see Fig. 5. This is due to transition from the valence bands (VBs) to the conduction bands (CBs) in Sn-s to Cl-p and Cl-p to Sn-p states. The critical energies show that the cubic and orthorhombic phases of $CsSnCl_3$ lie in the visible region. Many absorption peaks are observed in the spectra after these points from 4.7 to 15.2 and 4.5 to 20 eV for orthorhombic and cubic phase of $CsSnCl_3$, due to the transitions from Sn-s and Cl-p states of the VBs to Sn-p, Cl-p states of the CBs, shown in Fig. 3. The threshold points for cubic, orthorhombic and tetragonal phases of $CsSnBr_3$ are at 1.9, 1.2 and 1.8 eV, exploring their band gaps. These energies allow the permitted transitions from VBs of Sn-s and $Br_1$-p states to CBs of Sn-p and $Br_1$-p states for all phases of $CsSnBr_3$. Other peaks are observed from 3.4 to 20 eV for cubic, from 3.0 to 14.4 eV for tetragonal and from 2.6 to 15.6 eV for orthorhombic phases of $CsSnBr_3$, due to transitions from VBs of the Br-p and $Br_1$-p states to CBs of Sn-p and Cs-d states beyond and near the Fermi level. For different phases of $CsSnI_3$ the critical points are at 1.33, 1.75 and 1.20 eV due to transition from Sn-s, $I_2$-p and I-p states to Sn-p state,

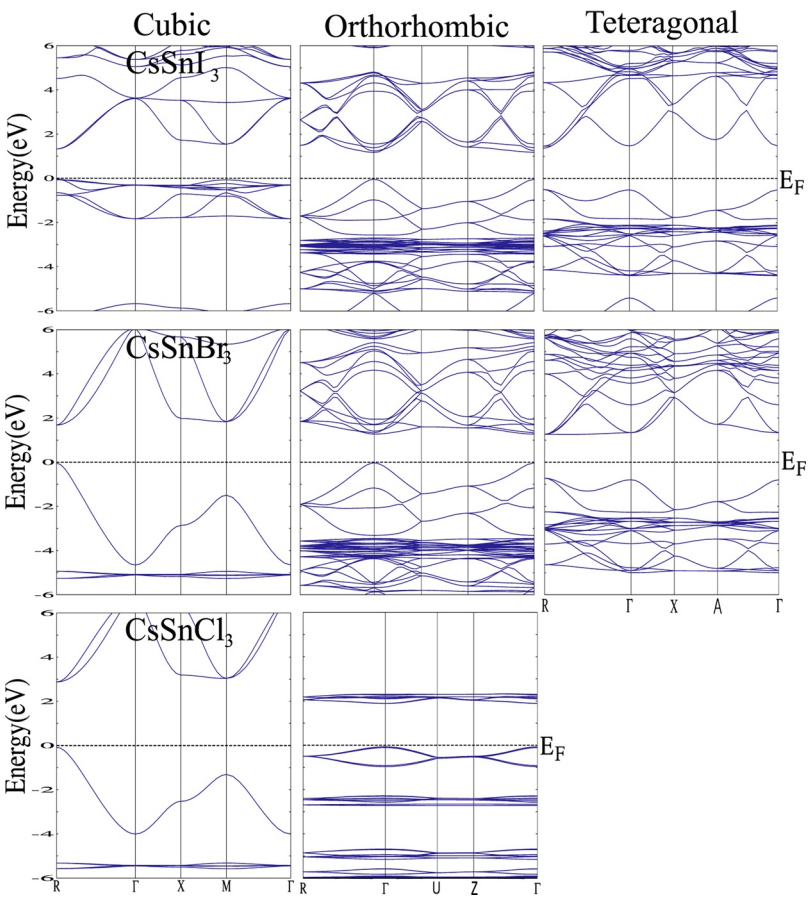


**Fig. 2.** Band structures of $CsSnX_3$ by nTB-mBJ.

**Table 4**
Comparison of presently calculated, experimental and other theoretically calculated bandgaps of $CsSnX_3$ (X = Cl, Br and I).

| Compounds | Phase | Present $E_g$ (eV) | | | Exp, $E_g$ (eV) | Others, $E_g$ (eV) |
|---|---|---|---|---|---|---|
| | | PBEsol | TB-mBJ | nTB-mBJ | | |
| $CsSnCl_3$ | Cubic | 0.642 | 1.428 | 2.93 | 2.9[b] | 0.950[a] |
| | | | | | | 2.99[b] |
| | Orthorhombic | 0.70 | 1.37 | 1.92 | – | – |
| | Cubic | 0.283 | 0.699 | 1.71 | 1.75[d,e] | 0.42[c] |
| | | | | | | 1.69[b] |
| $CsSnBr_3$ | Tetragonal | 2.20 | 2.3 | 1.96 | 1.8b | 0.40[c] |
| | | | | | | 1.98[b] |
| | Orthorhombic | 0.678 | 1.17 | 1.28 | 1.26[e] | – |
| | Cubic | 0.285 | 0.459 | 1.33 | – | 0.348[a] |
| | | | | | | 1.354[b] |
| $CsSnI_3$ | Tetragonal | 1.52 | 1.75 | 1.85 | – | 0.481[a] |
| | | | | | | 1.49[b] |
| | Orthorhombic | 0.495 | 0.635 | 1.20 | 1.3[b] | 0.561[a] |
| | | | | | | 1.3[b] |

a = [34], b = [24], c = [54], d = [1–55], e = [21].

revealing the optical band gaps. Many other peaks are seen from 2.5 to 17.5 eV due to transition from $I_1$-p and Sn-s states to Cs-d and Sn-p states respectively, shown in Fig. 3.

Ability of a material to pass the electromagnetic radiation is explored by Refractive index ($n(\omega)$). The calculated values of $n(\omega)$ for $CsSnX_3$ (X = Cl, Br and I) are explored in Fig. 6. The $n(0)$ are 1.7 and 1.6 for orthorhombic and cubic phases of $CsSnCl_3$, 1.8, 2.5 and 2.0 for cubic, orthorhombic and tetragonal phase of $CsSnBr_3$ and for different phases of $CsSnI_3$ their values are 2.35, 2.40 and 2.10 respectively, locating in the visible region. Beyond this limit, other peaks are observed at higher energies, locating in UV and far ultraviolet regions for all phases of $CsSnX_3$. Due to indirect transitions, $n(\omega)$ decreases below unity, and hence the speed of light at these energy limits becomes less than the group velocity and the medium changes to non-linear. Therefore, material losses the transparent character due to energy dissipations [41]. Moreover, the refractive index depends upon the crystallographic directions. Therefore, these materials exhibit the anisotropic nature in tetragonal and orthorhombic phases as shown in the Fig. 6.

Electron energy loss spectroscopy is used to know about the dielectric and metallic behaviors of a material [42]. Also we can obtain information about scattering (elastic or inelastic) of an electron using this technique [43,44]. The energy loss function $L(\omega)$ are explored for $CsSnX_3$, as shown in Fig. 7. Figure reveals that scattering of electrons is zero, when the band gap energy is greater than the photon energy and hence energy loss is zero. Beyond these energies maximum peaks are observed at 20.15 and 23.51 eV for orthorhombic and cubic phases of $CsSnCl_3$, at 22.5, 20 and 22 eV for cubic, orthorhombic and tetragonal phases of $CsSnBr_3$, and at 15.10, 20.55 and 18.32 eV for cubic, orthorhombic and tetragonal phases of $CsSnI_3$, respectively, showing inelastic scattering. Therefore, energy will be lost. At these frequencies plasma resonance takes place and such frequencies are termed as plasma frequencies. Above the plasma frequency the material is metallic, while it is dielectric below this frequency [41].

The sum rule ($N_{eff}$) explores the number of electrons used in optical transition and to find their strength. $N_{eff}$ is calculated and presented for different phases of $CsSnX_3$ in Fig. 8. This figure reveals that below the band gap energies the conduction bands are unoccupied by the electrons and at band gap energies their values raise, because some electrons can jump from VBs to CBs. When the photon energy is increased further, then $N_{eff}$ curve rises for each phase and finally these curves are saturated at 40 eV, see Fig. 8. At the saturated points the values of $N_{eff}$

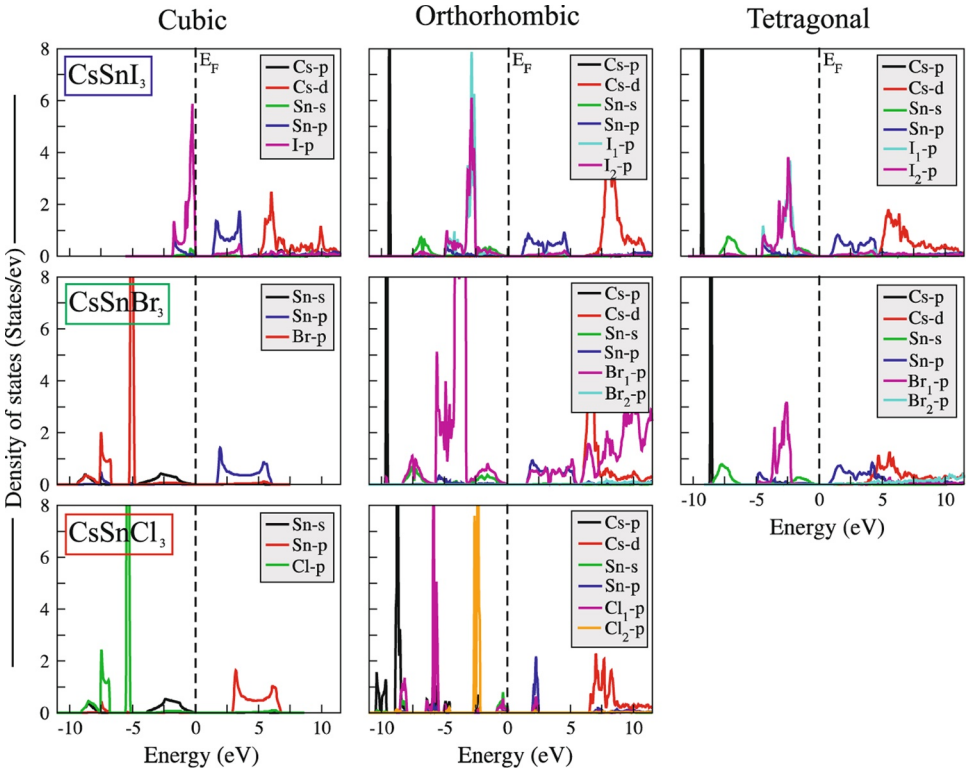


**Fig. 3.** Partial density of states for all phases of $CsSnX_3$ (X = Cl, Br and I).

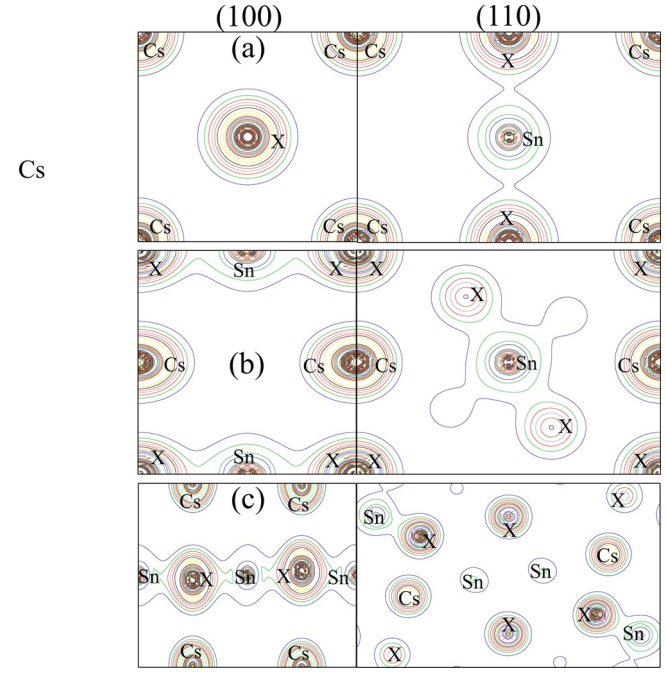


**Fig. 4.** Electronic charge densities for cubic (a), tetragonal (b) and orthorhombic (c) phases of $CsSnX_3$.

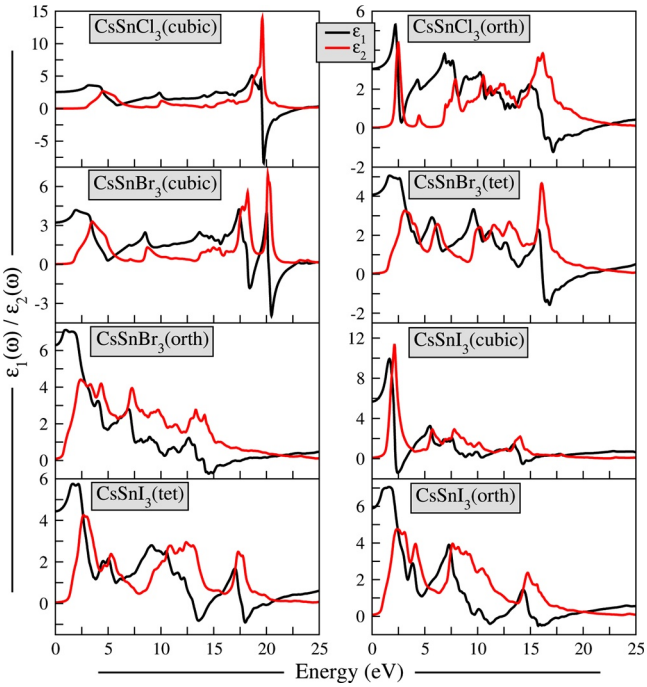


**Fig. 5.** Real and imaginary part of the complex dielectric function for different phases of $CsSnX_3$.

are 115 and 29 electrons for the orthorhombic and cubic phases of $CsSnCl_3$, 131, 70 and 32 electrons for the orthorhombic, tetragonal and cubic phases of $CsSnBr_3$, and 140, 72 and 38 electrons for the orthorhombic, tetragonal and cubic phases of $CsSnI_3$, respectively. This figure shows that the value of $N_{eff}$ decreases from orthorhombic to cubic phase and increases from Cl to Br to I. At different energies the oscillator strength decreases due to excitations of electrons loosely bound in p and d states to the conduction bands, see Fig. 8

## 5. Conclusions

In summary, the structural, electronic and optical properties of $CsSnX_3$ (X = Cl, Br, I) are explored using the FP-LAPW + lo method. It is concluded that the lattice constants and ground state energies are increased by replacing Cl with Br and I, while bulk moduli decrease. They have direct band gap nature, locating in visible region. The band gap decreases from Cl to Br and to I. The bonding nature reveals that strong

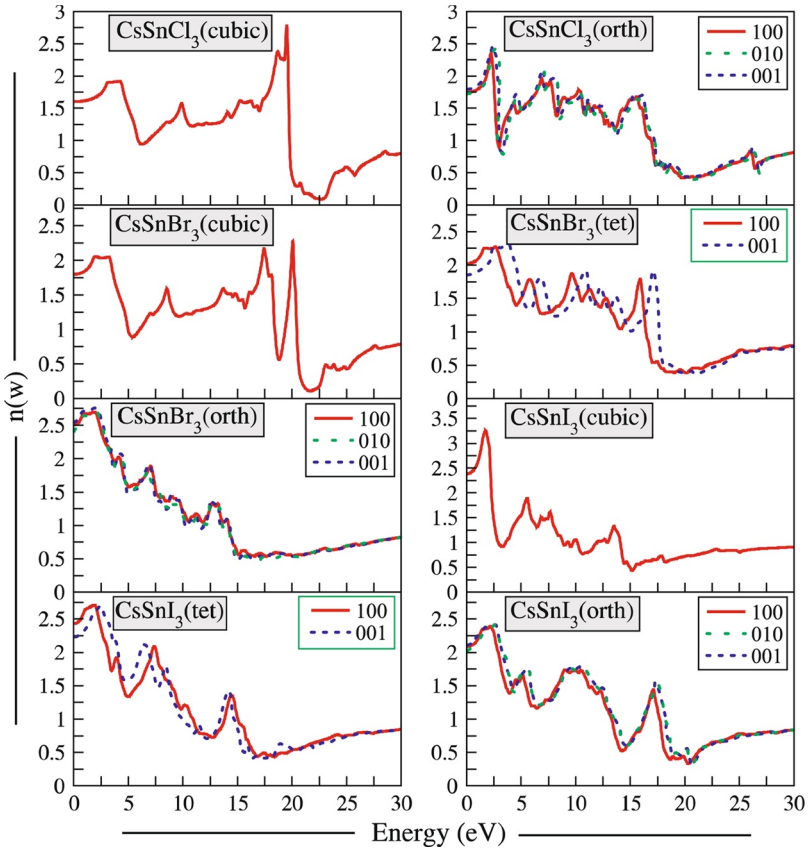


**Fig. 6.** Refractive indices for different phases of $CsSnX_3$.

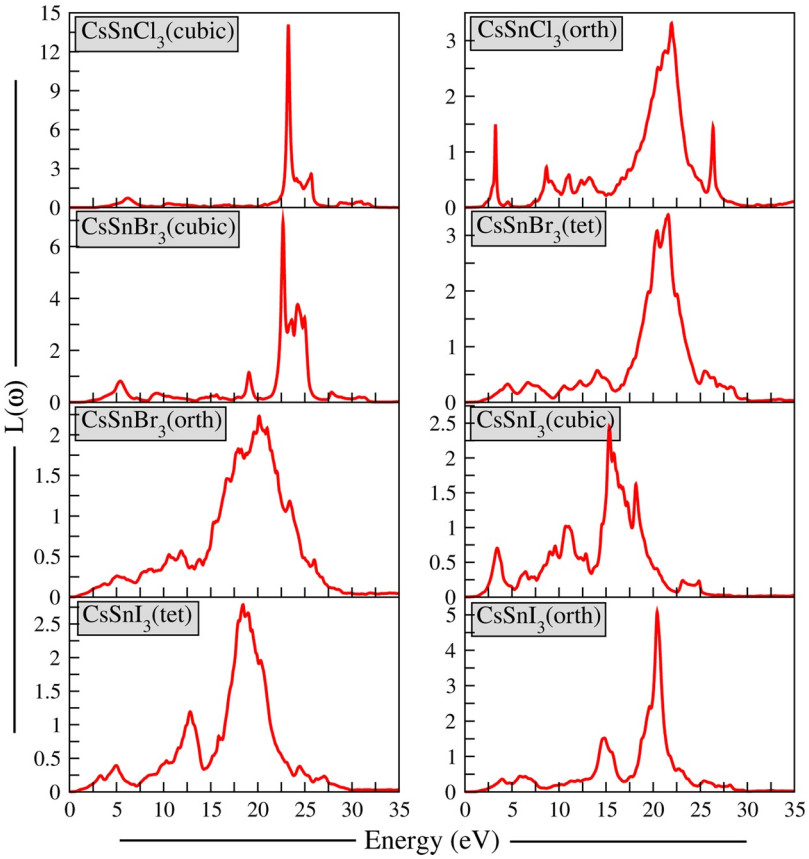


**Fig. 7.** Energy loss functions for different phases of $CsSnX_3$.

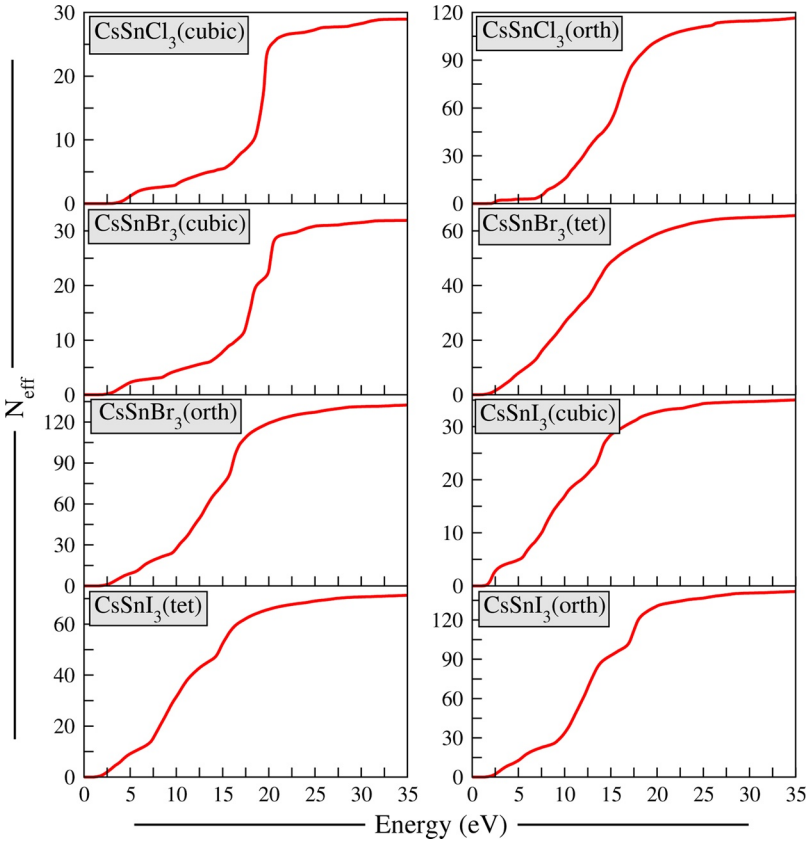


**Fig. 8.** Oscillator strength for different phases of $CsSnX_3$.

ionic bond exists between Cs and halide ions, while Sn and halide ions possess covalent bond nature. The imaginary part of dielectric function has many peaks, mainly from the transition of p and d states of Cs and halide ions from VB to CB of $CsSnX_3$ perovskites. The zero-frequency limit of the real part and refractive index increases from Cl to Br to I, show that the band gap decreases. We also concluded that the tetragonal and orthorhombic phase of these materials exhibit the anisotropic nature. The number of effective electrons increases from cubic to orthorhombic phase and from Cl to Br to I, revealing the excitations of loosely bound electrons from different p and d states of Cs and halide ions to the conduction band.

## Conflict of interest

None declared.

## Declaration of Competing Interest

The authors report no declarations of interest.

## Acknowledgement

We acknowledge the financial support from the Higher Education Commission of Pakistan (HEC), Project no. 20-3959/NRPU/R&D/HEC2014/234. and also thanks to Center for Computational Materials Science, University of Malakand Chakdara, Pakistan for computing support.

## References

[1] J. Weickert, R.B. Dunbar, H.C. Hesse, W. Wiedemann, L. Chmid, Adv. Mater. 23 (2011) 1810–1828.
[2] L.J. Chen, C. Lee, Y. Chuang, Z. Wu, C. Chen, J. Phys. Chem. Lett. 7 (2016) 5028–5035.
[3] H. Chen, S. Xiang, W. Li, H. Liu, L. Zhu, S. Yang, Sol. RRL 2 (1–23) (2018) 1700188.
[4] W. Ke, C.C. Stoumpos, M.G. Kanatzidis, Adv. Mater. 31 (1–31) (2019) 1803230.
[5] B. Parida, S. Yoon, S.M. Jeong, J.S. Cho, J. Kim, D. Kang, Sol. Energy Mater. Sol. Cells 204 (1–29) (2020) 110212.
[6] H. Siddiqui, Mater. Lett. 249 (2019) 99–103.
[7] J. Even, L. Pedesseau, C. Katan, M. Kepenekian, J.S. Lauret, D. Sapori, E. Deleporte, J. Phys. Chem. C 119 (2015) 1–49.
[8] J. Feng, B. Xiao, J. Phys. Chem. C 118 (2014) 19655–19660.
[9] I. Chung, J.H. Song, J. Im, J. Androulakis, C.D. Malliakas, H. Li, A.J. Freeman, J.T. Kenney, M.G. Kanatzidis, J. Am. Chem. Soc. 134 (2012) 8579–8587.
[10] J.F. Chabot, M. Cote, J.F. Briere, A.P.S. Meeting, Palais des Congres de Montreal Canada, March 22–26, 2004, American Physical Society, New York, 2004.
[11] A. Kaltzoglou, M. Antoniadou, D. Perganti, E. Siranidi, V. Raptis, K. Trohidou, V. Psycharis, A.G. Kontos, P. Falaras, Electrochim. Acta 184 (2015) 466–474.
[12] A. Kojima, K. Teshima, Y. Shirai, T. Miyasaka, J. Am. Chem. Soc. 131 (2009) 6050–6051.
[13] M. Mori, H. Saito, J. Phys. C: Solid State Phys. 19 (1986) 2391–2401.
[14] P. Xu, S. Chen, H.J. Xiang, X.G. Gong, S.H. Wei, Chem. Mater. 26 (2014) 6068–6072.
[15] F. Cao, W. Tian, M. Wang, L. Li, InfoMat 2 (2020) 577–584.
[16] Z. Hong, D. Tan, R.A. John, Y.K.E. Tay, Y.K.T. Ho, X. Zhao, T.C. Sum, N. Mathews, F. Garcia, H.S. Soo, iScience 16 (2019) 312–325.
[17] C.R. Kagan, D.B. Mitzi, C.D. Dimitrakopoulos, Science 286 (1999) 945–947.
[18] K. Shum, Z. Chen, J. Qureshi, C. Yu, J.J. Wang, W. Pfenninger, N. Vockic, J. Midgley, J.T. Kenney, Appl. Phys. Lett. 96 (2010) 221903–221905.
[19] D.E. Scaife, P.F. Weller, W.G. Fisher, J. Solid State Chem. 9 (1974) 308–314.
[20] P. Mauersberger, F. Huber, Acta Crystallogr. B 36 (1980) 683–684.
[21] S.J. Clark, C. Flin, J.D. Donaldson, J. Phys. Chem. Solids 42 (1981) 133–135.
[22] Q. Fan, B. Gee, Q. Xu, S. Pan, J. Peng, J. Ma, Z. Lin, Angew. Chem. Int. Ed. 59 (2020) 1030–1046.
[23] S. Ghosh, B. Pradhan, ChemNanoMat 5 (2019) 300–312.
[24] L. Huang, W.R.L. Lambrecht, Phys. Rev. B 88 (2013) 165203–165215.
[25] Y. Yuan, R. Xu, H. Xu, L. Wang, Proc. SPIE 9068 (2013) 906817–906821.
[26] L. Yu, W. Kassem, R. Bude, L. Divay, J. Amrit, S. Volz, 21st International Workshop on Thermal Investigations of ICs and Systems, Paris, September 30–October 2, 2015, IEEE, New Jersey, 2015.
[27] J. Islam, A.K.M.A. Hossain, RSC Adv. 10 (2020) 7817–7827.
[28] Z. Wu, Q. Zhang, B. Li, Z. Shi, K. Xu, Y. Chen, Z. Ning, Q. Mi, Chem. Mater. 31 (2019) 4999–5004.
[29] T. Xia, Y. Li, L. Huang, W. Ji, M. Yang, X. Zhao, ACS Appl. Mater. Interfaces 12 (2020) 18634–18641.
[30] P. Blaha, K. Shwarz, P. Sorantin, Comput. Phys. Commun. 59 (1990) 399–415.
[31] J.P. Perdew, Y. Wang, Phys. Rev. B 33 (1986) 8800–8802.
[32] F. Tran, P. Blaha, Phys. Rev. Lett. 102 (2009) 226401–226404.

[33] G. Rehman, M. Shafiq, Saifullah, R. Ahmad, S.J. Asadabadi, M. Maqbool, I. Khan, H.R. Aliabad, I. Ahmad, JEM 45 (2016) 3314–3323.
[34] I. Borriello, G. Cantele, D. Ninno, Phys. Rev. B 77 (1–9) (2008) 235214.
[35] Y. Pan, W.M. Guan, K.H. Zhang, Physica B 427 (2013) 17–21.
[36] F. Birch, Phys. Rev. 71 (1947) 809–824.
[37] T.H. Gfroerer, L.P. Priestley, F.E. Weindruch, M.W. Wanless, Appl. Phys. Lett. 80 (2002) 4570–4572.
[38] M.L. Benkhedir, M.S. Aida, A. Stesmans, G.J. Adriaenssens, J. Optoelectron. Adv. Mater. 7 (2005) 329–332.
[39] D. Penn, Phys. Rev. 128 (1962) 2093–2097.
[40] G. Murtaza, I. Ahmad, B. Amin, A. Afaq, M. Maqbool, J. Maqssod, I. Khan, M. Zahid, Opt. Mater. 33 (2011) 553–557.
[41] M. Ahmad, G. Rahman, L. Ali, M. Shafiq, R. Iqbal, R. Ahmad, T. Khan, S.J. Asadabadi, M. Maqbool, I. Ahmad, J. Alloys Compds. 705 (2017) 828–839.
[42] S. Loughin, R.H. French, L.K. Noyer, W.Y. Ching, Y.N. Xu, J. Phys. D 29 (1996) 1740–1750.
[43] H.A.R. Aliabad, S.M. Hosseini, A. Kompany, A. Youssefi, E.A. Kakhki, Phys. Stat. Sol. B 246 (2009) 1072–1081.
[44] R.F. Egerton, Rep. Prog. Phys. 72 (1–25) (2009) 016502.
[45] L. Lang, Y. Zhang, P. Xu, S. Chen, H.J. Xiang, X.G. Gong, Phys. Rev. B 92 (1–6) (2015) 075102.
[46] A. Majid, Y.S. Lee, Adv. Inform. Sci. Ser. Sci. 12 (2010) 118–127.
[47] R.A. Sinton, R.M. Swanson, IEEE 34 (1987) 1380–1389.
[48] L.Q. Jiang, J.K. Guob, H.B. Liua, M. Zhua, X. Zhoua, P. Wuc, C.H. Lia, J. Phys. Chem. Solids 67 (2006) 1531–1536.
[49] Q. Shen, Y. Ogomi, S.K. Das, S.S. Pandey, K. Yoshino, K. Katayama, H. Momose, T. Toyoda, S. Hayase, Phys. Chem. Chem. Phys. 15 (2013) 14370–14376.
[50] M.G. Brik, Solid State Commun. 151 (2011) 1733–1738.
[51] M.H. Kuok, E.L. Saw, C.T. Yap, Phys. Stat. Sol. 132 (1992) K89–K92.
[52] E.L. Silva, J.M. Skelton, S.C. Parker, A. Walsh, Phys. Rev. B 91 (1–12) (2015) 144107.
[53] A. Pivrikas, N.S. Sariciftci, G. Juska, R. Osterbacka, Res. Appl. 15 (2007) 677–696.
[54] J.C. Zheng, C.H.A. Huan, A.T.S. Wee, M.H. Kuok, Surf. Interface Anal. 28 (1999) 81–83.
[55] L. Peedikakkandy, P. Bhargava, RSC Adv. 47 (2016) 1–11.